LDHA- Mediated Histone Lactylation Promotes the Nonalcoholic Fatty Liver Disease Progression Through Targeting The METTL3/ YTHDF1/SCD1 m6A Axis

Juanjuan MENG[1,2], Caiwen YAN[2], Jinchun LIU[3]

[1]Shanxi Medical University, Yingze District, Taiyuan, Shanxi, China, [2]Department of Gastroenterology, Changzhi People's Hospital, Changzhi, Shanxi, China, [3]Department of Gastroenterology, First Hospital of Shanxi Medical University, Taiyuan, Shanxi, China

Received November 28, 2023
Accepted August 1, 2024

Summary

Nonalcoholic fatty liver disease (NAFLD) is characterized by elevated hepatic lipids caused by nonalcoholic factors, where histone lactylation is lately discovered as a modification driving disease progression. This research aimed to explore the role of histone 3 lysine 18 lactylation (H3K18lac) in NAFLD progression using a high-fat diet (HFD)-treated mouse model and free fatty acids (FFA)-treated L-02 cell lines. Lipids accumulation was screened via Oil Red O staining, real-time quantitative polymerase chain reaction (RT-qPCR), western blotting, and commercially available kits. Similarly, molecular mechanism was analyzed using immunoprecipitation (IP), dual-luciferase reporter assay, and RNA decay assay. Results indicated that FFA upregulated lactate dehydrogenase A (LDHA) and H3K18lac levels in L-02 cells. Besides, LDHA-mediated H3K18lac was enriched on the proximal promoter of methyltransferase 3 (METTL3), translating into an increased expression. Moreover, METTL3 or LDHA knockdown relieved lipid accumulation, decreased total cholesterol (TC) and triglyceride (TG) levels, and downregulated lipogenesis-related proteins in FFA-treated L-02 cell lines, in addition to enhancing the m6A and mRNA levels of stearoyl-coenzyme A desaturase 1 (SCD1). The m6A modification of SCD1 was recognized by YTH N6-methyladenosine RNA binding protein F1 (YTHDF1), resulting in enhanced mRNA stability. LDHA was found to be highly expressed in HFD-treated mice, where knocking down LDHA attenuated HFD-induced hepatic steatosis. These findings demonstrated that LDHA-induced H3K18lac promoted NAFLD progression, where LDHA-induced H3K18lac in METTL3 promoter elevated METTL3 expression, thereby promoting m6A methylation and stabilizing SCD1 via a YTHDF1-dependent manner.

Keywords

Nonalcoholic fatty liver disease • LDHA • METTL3 • YTHDF1 • Histone lactylation

Corresponding author

Jinchun Liu, Department of Gastroenterology, First Hospital of Shanxi Medical University, No.85 Jiefang South Road, Taiyuan, Shanxi 030000, China. E-mail: ljc2891@163.com

Introduction

Nonalcoholic fatty liver disease (NAFLD) is characterized by excessive lipid accumulation within the liver caused by nonalcoholic factors, translating into accumulation of lipid droplets in hepatocytes and liver enlargement, significantly affecting human health [1]. NAFLD pathogenesis is complex, where obesity, insulin resistance, microbiome alteration, diet, and genetic variations have been reported to be the primary factors [2]. Although NAFLD treatment is still challenging due to the unavailability of an approved therapeutic regimen, its clinical treatment is mainly focused on treating NAFLD-associated comorbidities, such as obesity, cardiovascular diseases, and diabetes mellitus type II. The treatment protocol for NAFLD is primarily focused on preventing hepatocyte oxidation, reducing the proinflammatory factors, and inhibiting lipid accumulation into the hepatocytes, but these options are often associated with side effects [3,4]. Therefore, it is of great importance to search for an effective NAFLD treatment.

Histones are octamers composed of H2A, H2B, H3, and H4 proteins, serving as the fundamental structural component of chromatin, surrounded by approximately 147 bp of DNA, connecting histone H1 to lock the DNA at both ends of the nucleosome [5]. Post-translational modifications of histones play a crucial role in regulating

gene expression. The alterations primarily take place at the N-terminus of histones, where a series of specific enzymes or binding proteins are used as "writers," "erasers," and "readers" to generate, eliminate, or recognize post-translational modifications to regulate "histone code" precisely [6,7]. Specific modification states can affect the binding affinity of histones to DNA, change chromosome conformation or recruit specific proteins to affect gene activity, thereby contributing to the onset and progression of various diseases [8,9]. Histone lactylation is a lately reported novel histone modification. Lactate can generate lactyl CoA, providing a lactyl group to the lysine tail of histone through acyltransferase, thus generating a histone modification called lysine lactylation (Klac) [10]. Histone lactylation plays a significant role in various pathological conditions, including cancer, infection, and tissue homeostasis [11,12]. Given that lactate is the final byproduct of glycolysis, numerous research studies have concentrated on histone lactylation in relation to cancer [13], [14], while one previous study reported graduate accumulation of lactate in the liver during NAFLD progression [15]. Nevertheless, the role of histone lactylation in NAFLD demands further investigations.

Epigenetic regulation's significance in metabolic diseases has garnered considerable attention in recent years. Epigenetic modification primarily consists of DNA methylation, RNA modification, and protein modification [16], which exists at the genomic and transcriptome levels and plays an important role in the biological mechanism of gene post-transcriptional regulation [17]. Among them, N6 methyladenine (m6A) is the predominant internal chemical modification found in mammalian cells [18], and m6A transcription can change the RNA secondary structure to promote the binding of regulatory proteins to affect their shearing, translation and degradation [19]. Currently, studies on m6A are primarily focused on tumors, with less attention paid to metabolic diseases [20]. The lactate has been found to induce histone lactylation on gene promoters, leading to the activation of gene expression [21]. Research has shown that histone lactylation takes place in the promoter region of m6A methylation-related enzymes, such as methyltransferase-like 3 (METTL3), translating into their abnormal upregulated expression, thereby regulating m6A modification and affecting disease progression [14,22]. Thus, we speculated that the histone lactylation-m6A methylation axis exists in NAFLD.

Therefore, this study aimed to investigate the role of lactate dehydrogenase A (LDHA)-mediated histone lactylation in NAFLD progression. It was hypothesized that lactylation of histone lysine 18 (H3K18lac) results in methyltransferase-like 3 (METTL3)-mediated elevation of stearoyl-coenzyme A desaturase 1 (SCD1) m6A levels, which in turn upregulated the SCD1 expression, further aggravating NAFLD progression.

Materials and Methods

NAFLD mouse model establishment

After adaptive feeding for one week, 20 C57BL/6J mice (male, 8-week-old, 18-22 g), provided by Shanghai Experimental Animal Center, Chinese Academy of Sciences (Shanghai, China), were randomly divided into standard-chow diet (SCD), high-fat diet (HFD), HFD + short hairpin RNA negative control (shNC), and LDHA knockdown, represented by the HFD + shLDHA groups, with 5 mice per group. The mice in the SCD group were fed with ordinary diet (the calories included 10 % fat, 60 % protein and 30 % carbohydrate), and the mice in the HFD group were fed with HFD diet (the calories included 60 % fat, 20 % protein and 20 % carbohydrate). For LDHA knockdown, 50 μL LDHA short hairpin RNA (shLDHA; GenePharma, Shanghai, China) were injected into the mice via the tail vein at $1x10^{11}$ PFU before the HFD treatment, i.e. the HFD + shLDHA group. Short hairpin RNA negative control (shNC; GenePharma) was also injected as the negative control, i.e. the HFD + shNC group. After 11 weeks of feeding, the mice were euthanized and dissected. Liver tissue samples were taken either to prepare liver homogenates for the detection of biochemical indices or for histopathological examination.

Cell culture and treatment

The human hepatocyte line L-02 was purchased from ATCC (Manassas, VA, USA) and placed in complete culture medium [the volume fraction of RPMI-1640 culture medium (Gibco, Grand Island, NY, USA) and fetal bovine serum (Gibco) were 90 % and 10 %, respectively] and cultured in an incubator with a volume fraction of 5 % CO_2 at 37 °C. The culture medium was changed every 24 hours. When the cells grew to the logarithmic phase (cell confluence > 80 %), they were digested and passaged with trypsin digestion solution. The cells after 5 passages were taken for NAFLD model establishment. The cultured L-02 cells were treated with 1 mM free fatty acids (FFA) for 24 h in standard growth medium to establish a NAFLD model. For lactate treatment, the cells were treated with 15 μM lactate in standard growth medium for 12 h.

Cell transfection

Short hairpin (sh) RNA targeting LDHA 1#/2#, shMETTL3 1#/2#, shYTHDF1 1#/2#, shIGF2BP1 1#/2#, shIGF2BP2 1#/2#, shIGF2BP3 1#/2#, shYTHDF2 1#/2#, shRNA negative control (shNC), LHDA overexpressed (oe) vector (oeLHDA), oeMETTL3, oeYTHDF1 and oe vector negative control (oeNC) were purchased from Guangzhou Ribobio (Guangzhou, China) and the cells were transfected with these plasmids using Lipofectamine® 2000 (Invitrogen, Carlsbad, CA, USA) according to the manufacturer's instructions. Twenty-four hours before transfection, L-02 cells were seeded into 6-well plates at a density of 1×10^5 cells/well, and fresh growing medium was replaced 6 h later. The cells were collected 48 h after transfection for subsequent analysis.

Real-time qPCR analysis

The qPCR was used to detect the expression level of related genes. Trizol reagent (Invitrogen) was used to extract total mRNA from liver tissue or L-02 cells, and cDNA was obtained after reverse transcription with a Reverse Transcription Kit (TransGen Biotech, Beijing, China). Real-time qPCR was conducted using a TransStart® Green qPCR SuperMix kit (TransGen Biotech) to detect the mRNA expressions. The expression level of target gene mRNA is expressed by $2^{-\triangle\triangle CT}$ with GAPDH as an internal reference. Primer sequences are shown in Table 1.

For the SCD1 mRNA stability determination, the cells were treated with 10 mg/L Actinomycin D for 0, 1, 2, 4, and 8 h. The RNA of the Actinomycin D-treated cells was extracted and used for qPCR to detect SCD1 expression.

Oil Red O staining

The L0-2 cells or the liver tissues were fixed with 4 % paraformaldehyde for 30 min. The cells were prepared into cell slides and covered with cover slides. The tissues were embedded in paraffin and were cut into sections with 6-μm thickness. Cell slices and tissue sections were stained with 2 ml of Oil Red O working solution (Sigma-Aldrich, St. Louis, MO, USA) for 10 min. After washing with 2 ml PBS, the cell and tissue sections were rinsed with 60 % isopropanol to decolorize. The sections were counterstained with haematoxylin for 1 min, followed by washing with 2 ml PBS again, and the formation of lipid droplets was observed under a microscope.

Western blot

Primary antibodies including anti-LDHA (ab52488, 1:5000), anti-SCD1 (ab236868, 1:800), anti-SREBP1 (ab28481, 1:800), anti-FAS (ab133619, 1:600), anti-METTL3 (ab195352, 1:1000), anti-METTL14 (ab309096, 1:1000) and anti-β-actin (ab8227, 1:2500) were purchased from Abcam (Cambridge, MA, USA). Anti-ACC (MA5-15025, 1:1200) was from Invitrogen. Anti-H3 (PTM-1001RM, 1:500) and anti-H3K18la (PTM-1427RM, 1:500) were obtained from PTM biolabs (Hangzhou, China). Biolabs Protein was extracted from cells and liver tissues by RIPA (Beyotime, Shanghai, China) reagents. The total protein concentration in lysate was determined with a BCA Protein Assay Kit (Beyotime). The proteins were separated by 10 % SDS-PAGE and electrotransferred to polyvinylidene fluoride membranes. The membranes were blocked with 5 % skim milk for 60 min and incubated with primary antibodies at 4°C overnight. Next day, the membranes were incubated with secondary antibody (horse radish peroxidase-conjugated goat anti-rabbit IgG, ab205718, 1:5000, Abcam) for 1.5 h. Subsequently, the protein band was determined by an ECL kit (Beyotime) using the ChemiDocXRS+ gel imaging system (Bio-Rad, Hercules, CA, USA).

M6A methylation level determination

The M6A content in total RNA of the cells were measured with EpiQuik M6A RNA Methylation Quantification Kit (AmyJet Scientific Inc, Wuhan, China). All operations were carried out in strict accordance with the requirements of the kit.

Table 1. Primer sequences used for qPCR

Factor	Forward (5'->3')	Reverse (5'->3'):
LDHA	ATGGCAACTCTAAAGGATCAGC	CCAACCCCAACAACTGTAATCT
SCD1	TTCTTGCGATACACTCTGGTGC	CGGGATTGAATGTTCTTGTCGT
GAPDH	CTCACCGGATGCACCAATGTT	CGCGTTGCTCACAATGTTCAT

Chromatin immunoprecipitation (ChIP) assay

ChIP assays were carried out with H3K18lac antibody. Rabbit IgG (ab313801, Abcam) was selected as the negative control. After crosslinking with 1 % formaldehyde for 10 min, the cells were collected and then quenched with glycine. Next, the cells were washed with pre-cold PBS, resuspended and sonicated. After that, the chromatin was incubated with antibodies and protein A/G beads at 4°C overnight. Finally, Chelex (Roche, Basel, Switzerland) was used to release the immunoprecipitated DNA and qPCR was conducted.

Determination of total cholesterol (TC), triglyceride (TG) and FFA levels

The levels of TC, TG and FFA in the cells were detected with using relative kits (Nanjing Jiangcheng Bioengineering Institute, Nanjing, China).

m6A RNA immunoprecipitation (MeRIP) assay

The m6A levels of SCD1 were analyzed using Magna MeRIP m6A Kit (Millipore, USA) according to the manufacturer's instructions. Briefly, the RNAs were incubated with 3μg of anti-m6A antibody and protein A/G magnetic beads (Thermo Scientific, Waltham, MA, USA) for 12 h at 4 ℃. And then the antibody-combined methylated RNA were incubated with the antibody in immunoprecipitation buffer with RNase and protease inhibitor. Finally, the interacting RNAs were isolated and m6A enrichment of SCD1 was detected using qRT-PCR.

RNA immunoprecipitation (RIP) assay

The Magna RIP RNA-Binding Protein Immunoprecipitation Kit (Millipore Billerica, MA, USA) was purchased to analyze the relationship between METTL3 and SCD1 (or FAS, ACC and SREBP1). Briefly, after transfected with METTL3, the cells were lysed using the RIP lysis buffer. Then the obtained cell extract was incubated with IgG antibody (ab313801, Abcam) and RIP buffer solution for 1h. Next, the cells were treated with magnetic beads. The protein was digested with proteinase K and the immunoprecipitated RNA was extracted. Finally, the RT-qPCR was performed to detect the SCD1, FAS, ACC and SREBP1 expressions.

Dual-luciferase reporter assay

Wild-type or mutant 3′-UTR of SCD1 (WT-SCD1 or MUT-SCD1) fragments were amplified and cloned into pGL3 vectors (Promega, Madison, WI, USA). The L-02 cells were seeded into 24-well plates and co-transfected with shRNAs (shMETTL3 or shYTHDF1) or overexpressed vectors (oeMETTL3 or oeYTHDF1) and recombinant plasmids using lipofectamine 2000. After 48 h, relative luciferase activity was detected using a dual-luciferase reporter assay system (Promega).

Hematoxylin and eosin (H&E) staining assay

Liver tissues were fixed in 10 % formalin and embedded in paraffin, and then cut into 4 μm thickness slices. The sections were stained with hematoxylin for 5 min and eosin for 1 min. A light microscope was used to view the results.

Masson trichrome staining

The paraffin sections were also used to conduct staining using the Masson trichrome staining kit (Solarbio, Beijing, China) according to the manufacturer's protocols. The results were captured using a light microscope.

Statistical analysis

In vitro experiments were performed on three bioreplicated samples, and *in vivo* experiments were performed on five bioreplicated samples. Each biological sample was repeated for three times. The error bars indicated standard deviation (SD). All data were in a normal distribution, and variance was similar between the groups that are being statistically compared. Statistical analyses were analyzed in GraphPad Prism 7. Statistical significance was determined by using unpaired Student t-test for two groups or one-way ANOVA when there are more than two groups. Differences in RNA stability between groups were analyzed using two-way ANOVA. $p < 0.05$ was considered significant.

Results

LDHA and H3K18lac were upregulated in FFA-treated cells

NAFLD cell lines were established using FFA, where results showed that FFA treatment induced elevated lactate (Fig. 1A) and LDHA (Fig. 1B) levels in a time-dependent manner, in addition to enhanced H3K18lac and LDHA protein levels in the L-02 cells (Fig. 1C).

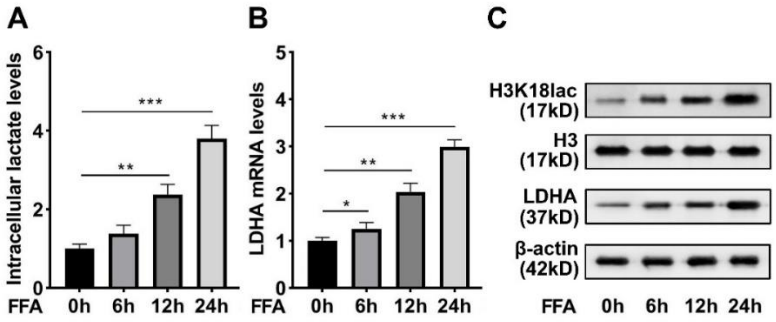

Fig. 1. LDHA and H3K18lac were upregulated in FFA-treated cells. (**A**) lactate and (**B**) LDHA levels in L-02 cells treated with FFA for different times. (**C**) The H3K18lac and LDHA levels in the FFA-treated L-02 cells. *p<0.05, **p<0.01, ***p<0.001.

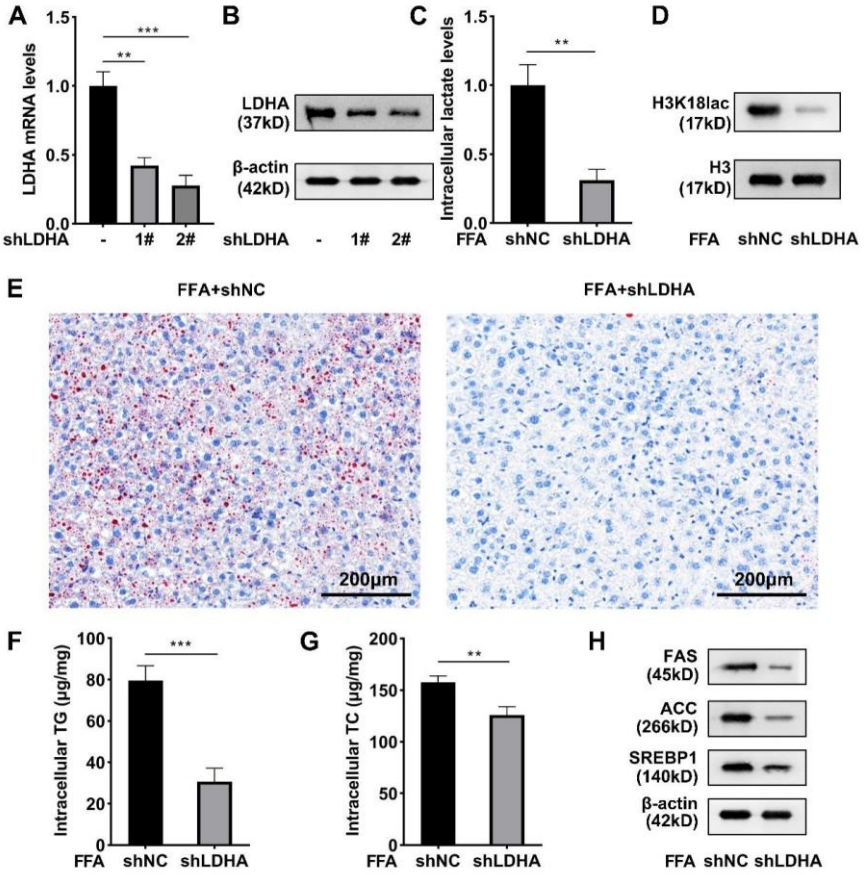

Fig. 2. Knockdown of LDHA prevented lipids accumulation *in vitro*. (**A-B**) Transfection efficiency of shLDHA, after shLDHA transfection. (**C**) The lactate levels and (**D**) H3K18lac in the FFA-treated L-02 cells were tested. (**E**) Oil Red O staining of the FFA-treated L-02 cells was performed. Scale bar: 200 μm. (**F**) The TG and (**G**) TC levels in the FFA-treated L-02 cells were assessed. (**H**) The protein levels of FAS, ACC and SREBP1 in the FFA-treated L-02 cells were detected. **p<0.01, ***p<0.001.

LDHA regulated the lipids accumulation in vitro

Post-shLDHA transfection demonstrated significantly decreased LDHA levels at mRNA (Fig. 2A) and protein (Fig. 2B) levels, while better transfection efficiency was observed with shLDHA 2#. Hence, it was then selected for subsequent experiments. Moreover, lactate levels (Fig. 2C) and H3K18lac (Fig. 2D) were dramatically downregulated post-shLDHA transfection. Similarly, Oil Red O staining revealed that knocking down LDHA relieved the excessive lipid accumulation in the FFA-treated L-02 cells (Fig. 2E), with significantly decreased TG (Fig. 2F) and TC (Fig. 2G), FAS, ACC, and SREBP1 protein levels (Fig. 2H). In addition, after LDHA overexpression (Fig. 3A–B), lactate (Fig. 3C) and H3K18la (Fig. 3D) levels were increased, lipid was accumulated (Fig. 3E), with the increased intracellular TG (Fig. 3F) and TC (Fig. 3G), as well as the upregulation of FAS, ACC, and SREBP1 levels (Fig. 3H), suggesting that overexpressing LDHA aggravated FFA-induced injury in L-02 cells.

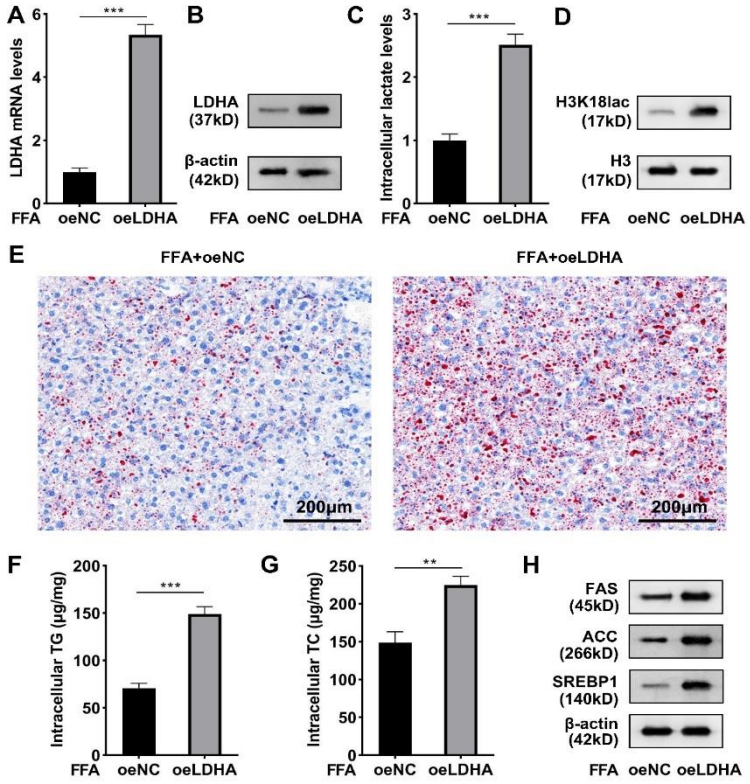

Fig. 3. Overexpression of LDHA promoted lipids accumulation *in vitro*. (**A-B**) Transfection efficiency of oeLDHA. The FFA-treated L-02 cells were transfected with oeLDHA. Then (**C**) the lactate levels, (**D**) H3K18lac, (**E**) Oil Red O staining (scale bar: 200 μm), (**F**) TG and (**G**) TC levels, and (**H**) the protein levels of FAS, ACC and SREBP1 were analyzed. **p<0.01, ***p<0.001.

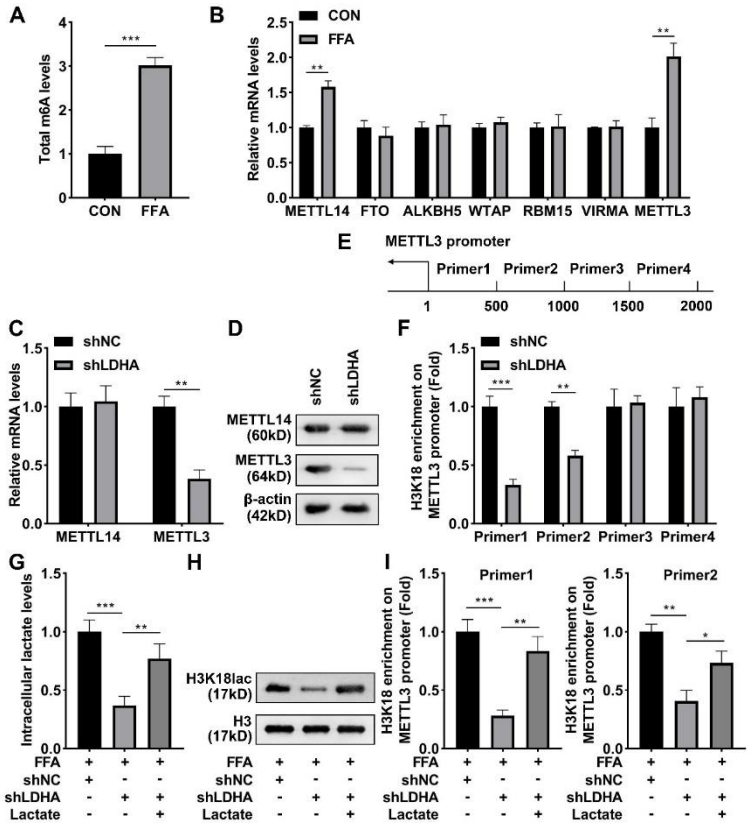

Fig. 4. LDHA upregulated METTL3 levels through H3K18 lactylation. (**A**) M6A levels in the FFA-treated L-02 cells. (**B**) The expression levels of m6A methylation-related enzymes in the FFA-treated L-02 cells. (**C**) The METTL3 and METTL4 mRNA and (**D**) protein levels in the FFA-treated and shLDHA transfected L-02 cells. (**E-F**) CHIP assay was conducted to analyze the H3K18 enrichment on the METTL3 promoter. (**G**) The lactate levels, (**H**) H3K18lac levels and (**I**) H3K18 enrichment on the METTL3 promoter in the FFA, shLDHA and lactate-treated L-02 cells. *p<0.05, **p<0.01, ***p<0.001.

LDHA upregulated METTL3 levels through H3K18 lactylation in the METTL3 promoter

The m6A levels were prominently enhanced in the FFA-treated L-02 cells (Fig. 4A). In contrast, analysis of expression levels of m6A methylation-related enzymes in the FFA-treated L-02 cells demonstrated enhanced METTL14 and METTL3 levels (Fig. 4B). However, post-LDHA knockdown, the METTL3 was downregulated. At

the same time, METTL14 showed no difference in mRNA (Fig. 4C) and protein levels (Fig. 4D). Furthermore, the H3K18lac enrichment on the METTL3 promoter was analyzed via CHIP assay. Results showed that H3K18 was enriched on the proximal promoter region of METTL3, and LDHA silencing prominently inhibited the occupancy of H3K18 (Figs. 4E–F). It was then proceeded by stimulating L-02 cells using lactate, and results showed that lactate treatment dramatically enhanced the lactate (Fig. 4G) and H3K18lac levels (Fig. 4H) compared to shLDHA-treated L-02 cells and restored the levels to their control shNC-transfected L-02 cells, while post-LDHA knockdown showed H3K18 enrichment on METTL3 promoter (Fig. 4I) in the FFA-treated L-02 cells.

Knockdown of METTL3 attenuated the lipids accumulation in vitro

A significantly decreased METTL3 at mRNA (Fig. 5A) and protein (Fig. 5B) levels were observed with post-shMETTL3 transfection, while excellent transfection efficiency was observed with shMETTL3 2# transfection, hence it was selected for subsequent experiments. Moreover, Oil Red O staining showed that METTL3 knockdown relieved the excessive lipid accumulation in the FFA-treated L-02 cells (Fig. 5C), while reduced TG (Fig. 5D) and TC (Fig. 5E) levels, along with downregulated FAS, ACC and SREBP1 protein levels (Fig. 5F) were observed with post-METTL3 knockdown FFA-treated L-02 cells.

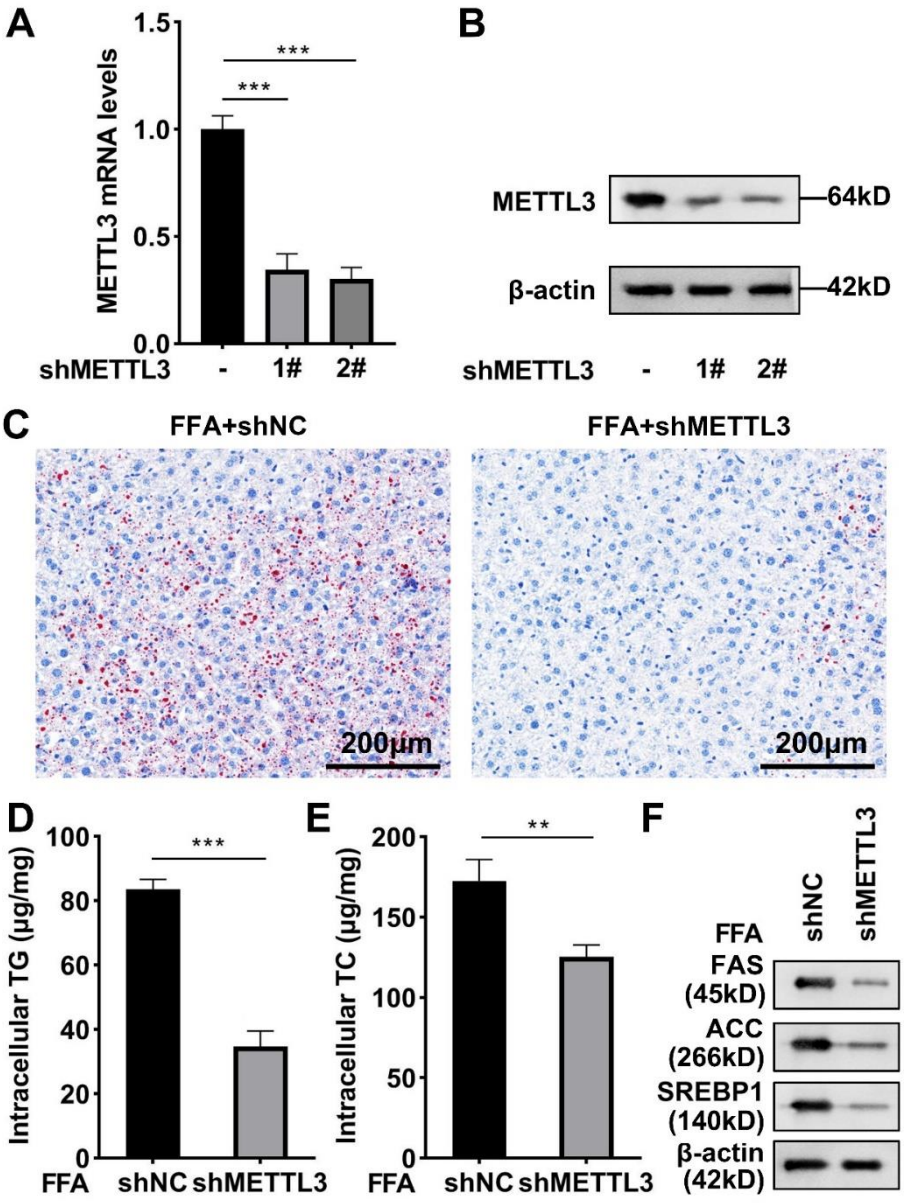

Fig. 5. Knockdown of METTL3 prevented lipids accumulation *in vitro*. (**A-B**) Transfection efficiency of shMETTL3. The FFA-treated L-02 cells were transfected with shMETTL3. Then, (**C**) Oil Red O staining (Scale bar: 200 μm), (**D**) TG and (**E**) TC levels, and (**F**) the protein levels of FAS, ACC and SREBP1 were analyzed. **p<0.01, ***p<0.001.

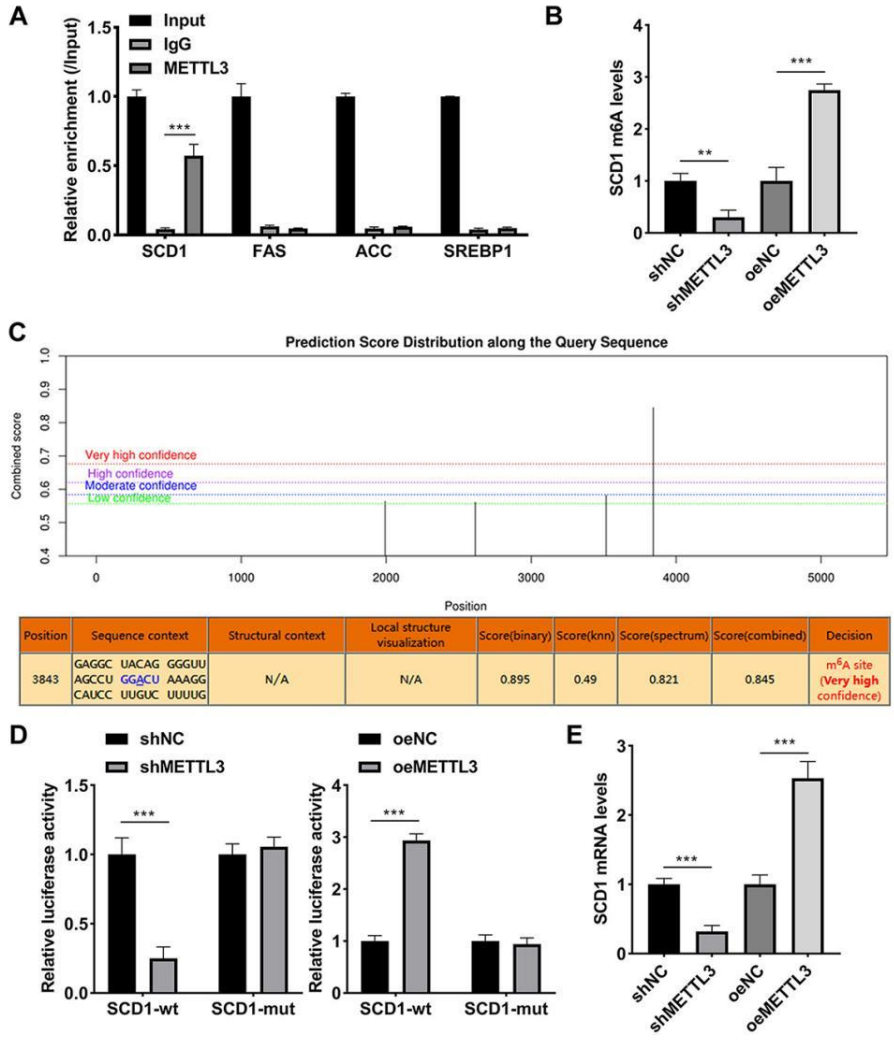

Fig. 6. METTL3 promoted the m6A and mRNA levels of SCD1. (**A**) The relationship between METTL3 and SCD1, FAS, ACC or SREBP1 was validated using RIP assay. (**B**) The m6A expression of SCD1 was assessed after METTL3 knockdown and overexpression. (**C**) The bioinformatic analysis of the methylation binding sites of SCD1. (**D**) The Luciferase activity of SCD1-wt and SCD1-mut were assessed after METTL3 knockdown and overexpression. (**E**) The mRNA expression of SCD1 was assessed after METTL3 knockdown and overexpression. **p<0.01, ***p<0.001.

METTL3 promoted the m6A and mRNA levels of SCD1

The RIP assay indicated that METTL3 was bound to SCD1 instead of FAS, ACC, and SREBP1 (Fig. 6A). The m6A levels of SCD1 were significantly decreased post-METTL3 knockdown, while opposite effects were observed with overexpressing METTL3 (Fig. 6B). Several methylation binding sites of SCD1 were found following bioinformatic analysis (Fig. 6C). Moreover, SCD1-wt luciferase activity was significantly decreased following METTL3 knockdown and increased post-METTL3 overexpression (Fig. 6D). Similarly, significantly reduced mRNA expression of SCD1 was observed following METTL3 knockdown and opposite results were obtained with METTL3 overexpression (Fig. 6E).

YTHDF1 elevated the SCD1 mRNA stability in an m6A-dependent manner

Previously discussed results showed that METTL3 induced significant changes in the m6A content and mRNA expressions of SCD1. It was then proceeded by investigating the m6A readers of SCD1, where following shRNAs transfection, the levels of m6A modification readers (IGF2BP1, IGF2BP2, IGF2BP3, YTHDF1, YTHDF1 and YTHDF2) were prominently reduced (Fig. 7A). Furthermore, post-shYTHDF1 transfection showed significantly decreased SCD1 levels (Fig. 7B), whereas YTHDF1 (Fig. 7C) and SCD1 (Fig. 7D) levels were dramatically elevated post-YTHDF1 overexpression, in addition to depleted luciferase activity of SCD1-wt following YTHDF1 knockdown and elevated post-YTHDF1 overexpression (Fig. 7E). The shYTHDF1 was found to deplete the mRNA stability of SCD1 and was enhanced by oeYTHDF1 (Fig. 7F). Finally, it was found that YTHDF1 knockdown reversed the elevated METTL3 overexpression induced SCD1 mRNA (Fig. 7G) and protein (Fig. 7H) levels.

LDHA knockdown alleviated the NAFLD progression in vivo

Male mice at the age of 8-week-old were fed with

HFD to established an *in vivo* mouse model. The results indicated that FFA (Fig. 8A), TG (Fig. 8B) and TC (Fig. 8C) levels, and FAS, ACC and SREBP1 protein levels (Fig. 8D) were significantly increased in the liver tissues, in addition to LDHA mRNA (Fig. 8E) and protein (Fig. 8F) levels. Then, to investigate the role of LDHA *in vivo*, shNC and shLDHA were injected into the mice through the tail vein. Mice fed with HFD as well as the HFD+shNC group displayed significantly increased body weight (Fig. 9A), liver weight (Fig. 9B), and adipose tissue weight (Fig. 9C) compared to their controls fed with SCD. However, their weights were decreased in the HFD+shLDHA group, compared with the HFD+shNC group, especially the liver weight, was comparable to the SCD group. Additionally, knocking down LDHA translated into significantly reduced FFA (Fig. 9D), TG (Fig. 9E) and TC (Fig. 9F) levels, and FAS, ACC and SREBP1 protein levels (Fig. 9H) in the liver tissues of the HFD-treated mice.

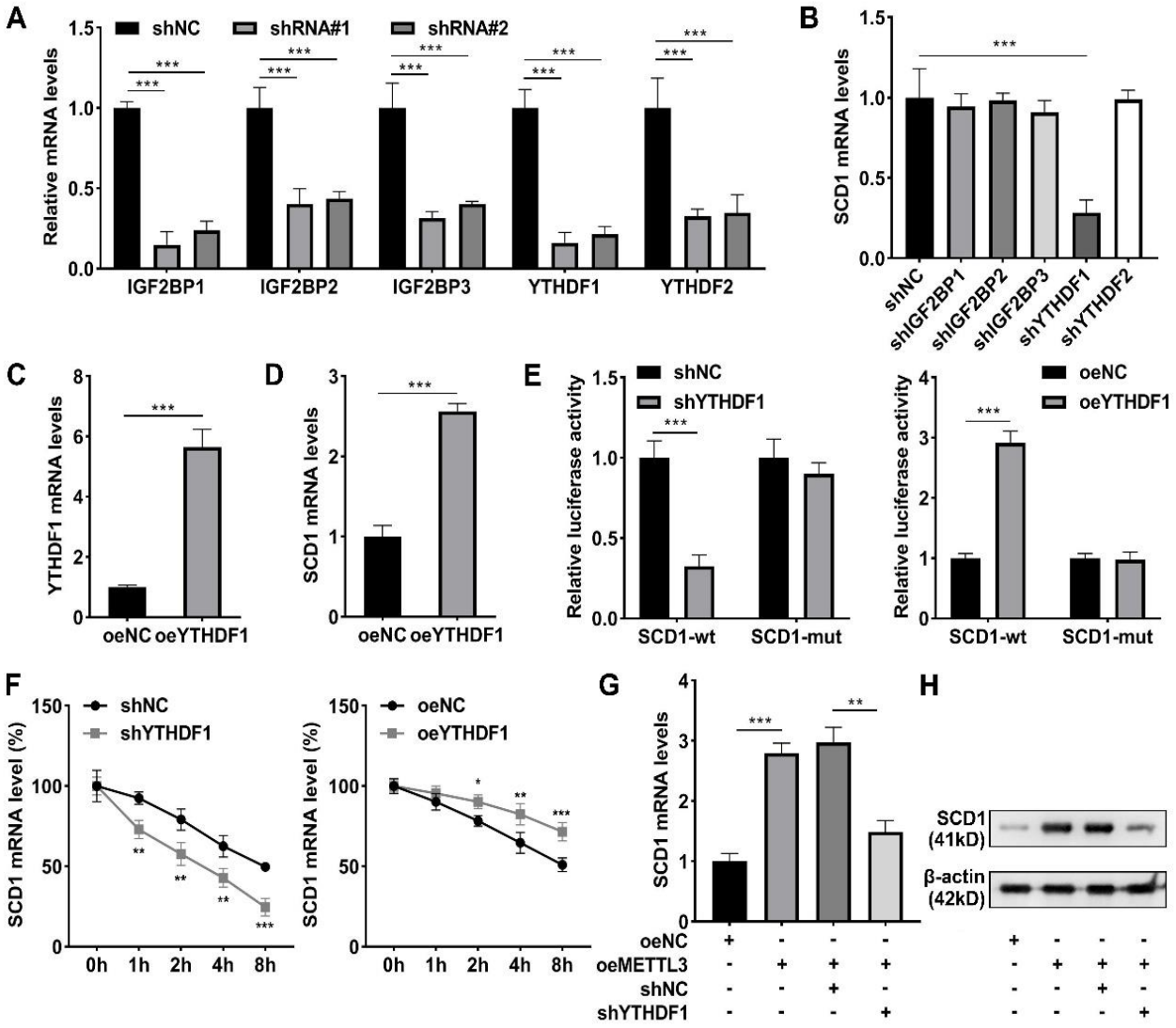

Fig. 7. YTHDF1 elevated the SCD1 mRNA stability in an m6A-dependent manner. (**A**) Validation of transfection efficiency. (**B**) SCD1 levels were assessed after the knockdown of m6A readers. (**C**) The YTHDF1 levels and (**D**) SCD1 levels were determined after YTHDF1 overexpression. (**E**) The Luciferase activity of SCD1-wt and SCD1-mut was assessed after YTHDF1 knockdown and overexpression. (**F**) The stability of SCD1 was assessed after YTHDF1 knockdown and overexpression. (**G**) The mRNA and (H) protein levels of SCD1 were determined after oeMETTL3 and shYTHDF1 transfection. *p<0.05, **p<0.01, ***p<0.001.

Oil Red O staining showed an accumulation of excessive lipids in the liver of the HDF-treated mice, which was relieved by knocking down LDHA (Fig. 9G). H&E staining results indicated that HFD led to liver pathological injury in mice, and LDHA knockdown attenuated pathological damage in HFD mice (Fig. 9G). Masson trichrome staining results showed that HFD caused the increase of collagen fibers in the liver, compared with the SCD group. Nevertheless, the collagen fibers were lower in the HFD + shLDHA group than that in HFD + shNC group (Fig. 9G). Moreover, METTL3 and SCD1 protein levels were increased in the liver of HFD mice, while silencing of LDHA decreased their levels in HFD mice (Fig. 9I).

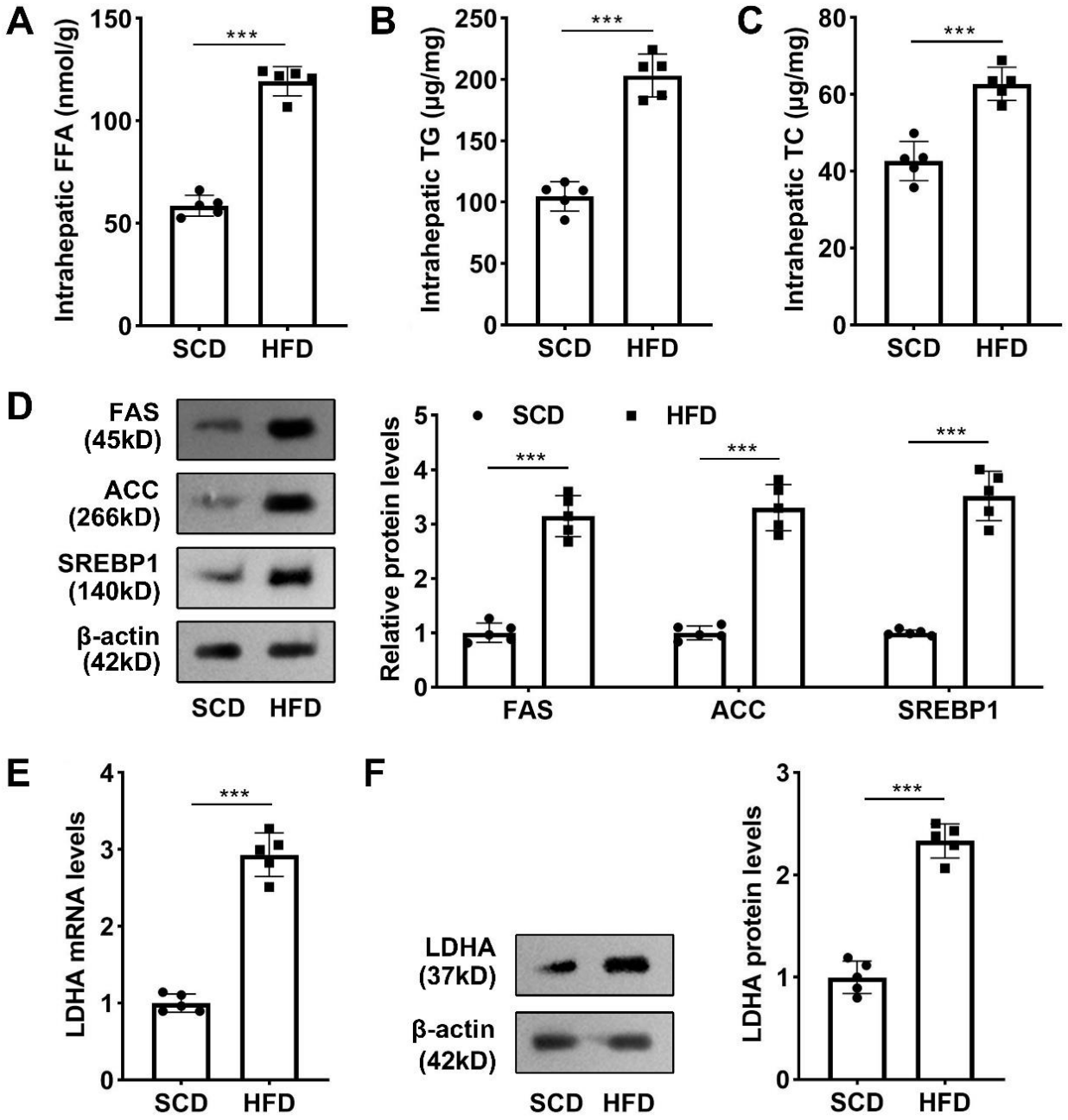

Fig. 8. The establishment of the NAFLD model *in vivo*. (**A**) The FFA, (**B**) TG, (**C**) TC, and (**D**) protein levels of FAS, ACC and SREBP1 in the HFD-treated mice were analyzed. The (**E**) mRNA and (**F**) protein levels of LDHA in the HFD-treated mice were analyzed. ***p<0.001.

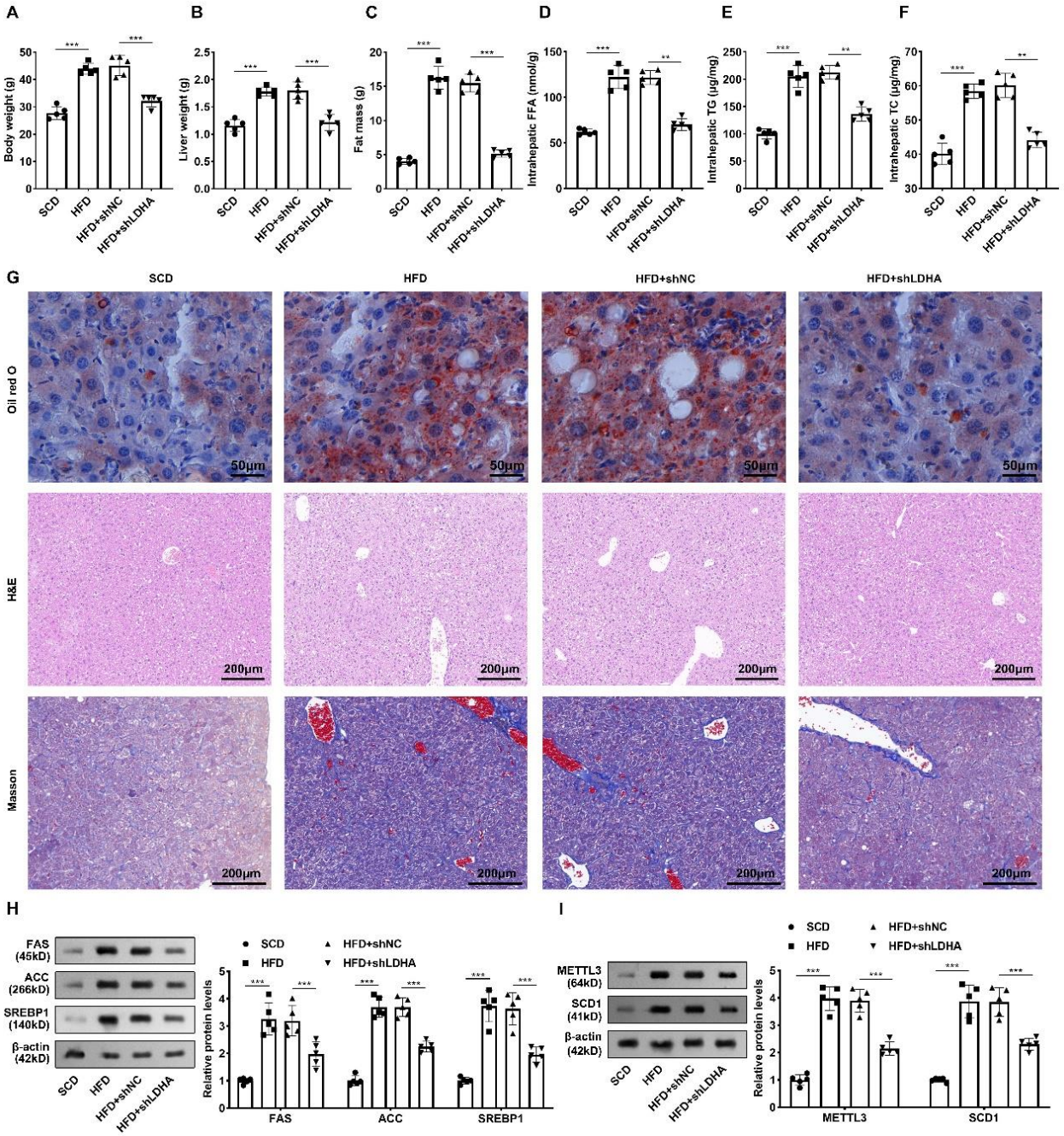

Fig. 9. LDHA knockdown relieved the NAFLD progression *in vivo*. The (**A**) body weight, (**B**) liver weight, and (**C**) adipose tissue weight of mice in each group were quantified. The (**D**) FFA, (**E**) TG and (**F**) TC levels in the HFD-treated mice after LDHA knockdown were analyzed. (**G**) Represent images of Oil Red O, H&E, Masson trichrome staining of the liver in the HDF-treated mice. The scale bar for Oil Red O staining is 50 μm, and those for H&E and Masson trichrome staining is 200 μm. (**H-I**) The protein levels of FAS, ACC, SREBP1, METTL3 and SCD1 in the livers of the HDF-treated mice after LDHA knockdown were analyzed. **p<0.01, ***p<0.001.

Discussion

Our results demonstrated that LDHA was up-regulated in FAA-treated L-02 cells and HFD-fed mice, along with elevated H3K18lac levels in FAA-treated L-02 cells. Additionally, LDHA-mediated H3K18lac in the METTL3 promoter enhanced the m6A levels of SCD1. Besides, METTL3 epigenetically enhanced the SCD1 expression in an m6A-YTHDF1-dependent manner.

LDHA plays an important role in glycolytic metabolism, primarily converting pyruvate into lactate and nicotinamide adenine dinucleotide (NADH) into diphosphopyridine nucleotide (NAD+) [23]. LDHA is located in the short arm of chromosome 11 [24], with a coding sequence of about 1000 bp and a relative molecular weight of about 35 kDa [25]. Several studies have

demonstrated that LDHA is abnormally highly expressed in various diseases and is closely associated with cell proliferation, migration, nuclear entry regulation, and other biological activities [26,27]. Lactate production in glycolysis significantly promotes cell invasion and the triggering of immune escape [28]. Recent studies have shown that elevated LDHA levels lead to increased lactate production, resulting in histone lactylation. It has been reported that LDHA levels were gradually increased during osteogenic differentiation, inducing histone lactylation mark enrichment on the JunB promoter [29], while hypoxia was found to inhibit LDHA activity resulting in downregulated lactate, suppressed histone lactylation, thereby impairing mouse embryo development [30]. Histone lactylation is a double-edged sword in the development of various diseases since increased lactate levels have been observed during NAFLD progression in the liver of patients [15]. Additionally, prior research has shown that decreasing hepatic steatosis results in reduced LHDA expression and lactate concentration in mice [31]. Hence, it was speculated that increased LDHA or lactate might regulate lactylation in NAFLD. Additionally, the lactylation of fatty acid synthase modulated by mitochondrial pyruvate carrier 1 (MPC1) was also found to inhibit liver lipid accumulation in NAFLD [32], suggesting the involvement of lactylation NAFLD. However, the role of histone lactylation in NAFLD has not been reported yet. Our results demonstrated that LDHA-induced H3K18lac enhanced the TC and TG levels, as well as related indicators of fatty acid synthesis (SCD1, FAS and SREBP1). This could be a contributing factor to the development of NAFLD. However, the specific mechanism of histone lactylation in NAFLD needs to be further explored.

Histone lactylation has previously been reported to be closely related to the m6A methylation modification in the ocular melanoma progression [33], which has also been reported for NAFLD progression. The upregulation of ACLY and SCD1 levels in the NAFLD model was demonstrated to be induced by METTL3/14 mediated excessive m6A modification, elevating TG and TC production in addition to accumulation of lipid droplets [34]. Our results demonstrated that LDHA-mediated H3K18lac was not only enriched on the proximal promoter of METTL3 but also increased its expression. Similarly, knocking down METTL3 prevented the TC and TG production, along with SCD1, FAS, and SREBP1 levels in the FFA-treated L-02 cells, implying that overly expressed LDHA participated in the NAFLD by regulating METTL3-mediated m6A methylation modification *via* H3K18lac. Similarly, upregulated METTL3 was reported in NAFLD mice and FFA-treated hepatocytes, which were directly bound to Rubicon, regulating its mRNA expression through the m6A methylation modification [35]. Thus, it was speculated whether METTL3 could promote the development of NAFLD by regulating the expression of SCD1 since SCD1 has been reported to play a vital role in fatty acid metabolism, serving as a key enzyme in monounsaturated fatty acid synthesis [36], primarily catalyzing stearoyl- and palmitoyl- to form oleoyl and palmitoyl CoA, which acts as substrates preferentially used in the biosynthesis of membrane phospholipids, TG and TC. A lack of oleoyl and palmitoyl CoA will translate into lipid esterification obstacles, change the lipid composition of cell membranes, and affect cellular functions [37,38]. Thus, the normal expression of SCD1 has a positive regulatory effect on fatty acid metabolism. Our results showed that METTL3 was bound to SCD1 and enhanced its levels through the m6A methylation modification.

Different m6A readers have been reported to determine the fate of mRNA generation and degradation during the process of m6A methylation modification [39], where m6A readers recognize and bind m6A modification sites to play the corresponding physiological role [40]. YTHDF1, as a member of m6A readers, is demonstrated to guard m6A-modified mRNAs from decay [41], and recognizes m6A modification of the target genes, thus regulating their expression. Lin *et al.* [42] reported forkhead box O3 (FOXO3) as a key downstream target of METTL3, where m6A levels were regulated by METTL3. Additionally, the recognition of m6A modification and regulation of the stability of FOXO3 was dependent on YTHDF1 in the hepatocellular carcinoma progression. In NAFLD, YTHDF1, as a partner of METTL3, was demonstrated to interact with the m6A-marked Rubicon mRNA and enhance Rubicon stability [35]. Similarly, in this study, the interaction between SCD1 and YTHDF1 was demonstrated using the luciferase report assay, and knocking down YTHDF1 was found to decrease SCD1 stability and neutralize the oeMETTL3 effects on SCD1 levels.

In conclusion, our study revealed that high levels of LDHA-induced histone lactylation accelerated the progression of NAFLD. Mechanistically, LDHA-induced H3K18lac enhanced the METTL3 levels in the proximal promoter of METTL3, which further epigenetically enhanced the SCD1 expression via an m6A-YTHDF1-

dependent manner.

Ethical approval

This study protocol was approved by the Ethics Committee of Changzhi People's Hospital. All experiments were performed in accordance with European Guidelines on Laboratory Animal Care.

Author contributions

Jinchu Liu: Conceptualization, Methodology; Caiwen Yan: Data curation, Writing- Original draft preparation; Juanjuan Meng: Writing- Reviewing and Editing.

Conflict of Interest

There is no conflict of interest.

References

1. Abdelmalek MF. Nonalcoholic fatty liver disease: another leap forward. Nature reviews. Gastroenterol Hepatol 2021;18:85-86. https://doi.org/10.1038/s41575-020-00406-0
2. Ko E, Yoon EL, Jun DW. Risk factors in nonalcoholic fatty liver disease. Clin Mol Hepatol 2023;29(Suppl):S79-S85. https://doi.org/10.3350/cmh.2022.0398
3. Makri E, Goulas A, Polyzos SA. Epidemiology, pathogenesis, diagnosis and emerging treatment of nonalcoholic fatty liver disease. Arch Med Res 2021;52:25-37. https://doi.org/10.1016/j.arcmed.2020.11.010
4. Singh S, Osna NA, Kharbanda KK. Treatment options for alcoholic and non-alcoholic fatty liver disease: A review. World J Gastroenterol 2017;23:6549-6570. https://doi.org/10.3748/wjg.v23.i36.6549
5. Zhang Y, Sun Z, Jia J, Du T, Zhang N, Tang Y, Fang Y, Fang D. *Overview of histone modification. First* Online: 07 November 2020. 2020;1283:1-16. https://doi.org/10.1007/978-981-15-8104-5_1
6. Andrés M, García-Gomis D, Ponte I, Suau P, Roque A. Histone H1 post-translational modifications: update and future perspectives. International J Mol Sci 2020;21:5941. https://doi.org/10.3390/ijms21165941
7. Tolsma TO, Hansen JC, Gilbert N, Allan J. Post-translational modifications and chromatin dynamics. Essays Biochem 2019;63:89-96. https://doi.org/10.1042/EBC20180067
8. Hamam HJ, Palaniyar N. Post-Translational Modifications in NETosis and NETs-Mediated Diseases. Biomolecules 2019;9. https://doi.org/10.3390/biom9080369
9. Singh G, Singh V, Schneider JS. Post-translational histone modifications and their interaction with sex influence normal brain development and elaboration of neuropsychiatric disorders. Biochim Biophys Acta Mol Basis Dis 2019;1865:1968-1981. https://doi.org/10.1016/j.bbadis.2018.10.016
10. Zhang D, Tang Z, Huang H, Zhou G, Cui C, Weng Y, Liu W, Kim S, Lee S, Perez-Neut M, Ding J, Czyz D, Hu R, Ye Z, He M, Zheng YG, Shuman HA, Dai L, Ren B, Roeder RG, Becker L, Zhao Y. Metabolic regulation of gene expression by histone lactylation. Nature (London) 2019;574(7779):575-580. https://doi.org/10.1038/s41586-019-1678-1
11. Schvartzman JM, Thompson CB, Finley LWS. Metabolic regulation of chromatin modifications and gene expression. J Cell Biol 2018;217:2247-2259. https://doi.org/10.1083/jcb.201803061
12. Trefely S, Doan MT, Snyder NW. Crosstalk between cellular metabolism and histone acetylation. Methods Enzymol 2019;626:1-21. https://doi.org/10.1016/bs.mie.2019.07.013
13. Bhagat TD, Von Ahrens D, Dawlaty M, Zou Y, Baddour J, Achreja A, Zhao H, Yang L, Patel B, Kwak C, Choudhary GS, Gordon-Mitchell S, Aluri S, Bhattacharyya S, Sahu S, Bhagat P, Yu Y, Bartenstein M, Giricz O, Suzuki M, Sohal D, Gupta S, Guerrero PA, Batra S, Goggins M, Steidl U, Greally J, Agarwal B, Pradhan K, Banerjee D, Nagrath D, Maitra A, Verma A. Lactate-mediated epigenetic reprogramming regulates formation of human pancreatic cancer-associated fibroblasts. Elife 2019;8. https://doi.org/10.7554/eLife.50663
14. Yu J, Chai P, Xie M, Ge S, Ruan J, Fan X, Jia R. Histone lactylation drives oncogenesis by facilitating m(6)A reader protein YTHDF2 expression in ocular melanoma. Genome Biol 2021;22:85. https://doi.org/10.1186/s13059-021-02308-z
15. Wang T, Chen K, Yao W, Zheng R, He Q, Xia J, Li J, Shao Y, Zhang L, Huang L, Qin L, Xu M, Zhang Z, Pan D, Li Z, Huang F. Acetylation of lactate dehydrogenase B drives NAFLD progression by impairing lactate clearance. J Hepatol 2021;74:1038-1052. https://doi.org/10.1016/j.jhep.2020.11.028

16. Chen Y, Hong T, Wang S, Mo J, Tian T, Zhou X. Epigenetic modification of nucleic acids: from basic studies to medical applications. Chem Soc Rev 2017;46:2844-2872. https://doi.org/10.1039/C6CS00599C
17. Zhao LY, Song J, Liu Y, Song CX, Yi C. Mapping the epigenetic modifications of DNA and RNA. Protein Cell 2020;11:792-808. https://doi.org/10.1007/s13238-020-00733-7
18. Zhong H, Tang HF, Kai Y. N6-methyladenine RNA Modification (m(6)A): An Emerging Regulator of Metabolic Diseases. Curr Drug Targets 2020;21:1056-1067. https://doi.org/10.2174/1389450121666200210125247
19. Huang W, Chen T, Fang K, Zeng Z, Ye H, Chen Y. N6-methyladenosine methyltransferases: functions, regulation, and clinical potential. J Hematol Oncol 2021;14:1-117. https://doi.org/10.1186/s13045-021-01129-8
20. Yang J, Chen J, Fei X, Wang X, Wang K. N6-methyladenine RNA modification and cancer. Oncol Lett 2020;20:1504-1512. https://doi.org/10.3892/ol.2020.11739
21. Zhang D, Tang Z, Huang H, Zhou G, Cui C, Weng Y, Liu W, Kim S, Lee S, Perez-Neut M, Ding J, Czyz D, Hu R, Ye Z, He M, Zheng YG, Shuman HA, Dai L, Ren B, Roeder RG, Becker L, Zhao Y. Metabolic regulation of gene expression by histone lactylation. Nature 2019;574(7779):575-580. https://doi.org/10.1038/s41586-019-1678-1
22. Xiong J, He J, Zhu J, Pan J, Liao W, Ye H, Wang H, Song Y, Du Y, Cui B, Xue M, Zheng W, Kong X, Jiang K, Ding K, Lai L, Wang Q. Lactylation-driven METTL3-mediated RNA m(6)A modification promotes immunosuppression of tumor-infiltrating myeloid cells. Mol Cell 2022;82:1660-1677. https://doi.org/10.1016/j.molcel.2022.02.033
23. Read JA, Winter VJ, Eszes CM, Sessions RB, Brady RL. Structural basis for altered activity of M- and H-isozyme forms of human lactate dehydrogenase. Proteins, structure, function, and bioinformatics 2001;43:175-185. https://doi.org/10.1002/1097-0134(20010501)43:2<175::AID-PROT1029>3.0.CO;2-%23
24. Feng Y, Xiong Y, Qiao T, Li X, Jia L, Han Y. Lactate dehydrogenase A: A key player in carcinogenesis and potential target in cancer therapy. Cancer Med, 2018;7(12):6124-6136. https://doi.org/10.1002/cam4.1820
25. Jafary F, Ganjalikhany MR, Moradi A, Hemati M, Jafari S. Novel peptide inhibitors for lactate dehydrogenase A (LDHA): A survey to inhibit LDHA activity via disruption of protein-protein interaction. Sci Rep 2019;9:4686. https://doi.org/10.1038/s41598-019-38854-7
26. Liu Y, Guo JZ, Liu Y, Wang K, Ding W, Wang H, Liu X, Zhou S, Lu XC, Yang HB, Xu C, Gao W, Zhou L, Wang YP, Hu W, Wei Y, Huang C, Lei QY. Nuclear lactate dehydrogenase A senses ROS to produce alpha-hydroxybutyrate for HPV-induced cervical tumor growth. Nat Commun 2018;9:4429. https://doi.org/10.1038/s41467-018-06841-7
27. Sheppard S, Santosa EK, Lau CM, Violante S, Giovanelli P, Kim H, Cross JR, Li MO, Sun JC. Lactate dehydrogenase A-dependent aerobic glycolysis promotes natural killer cell anti-viral and anti-tumor function. Cell Rep 2021;35:109210. https://doi.org/10.1016/j.celrep.2021.109210
28. Sun L, Li J, Yan W, Yao Z, Wang R, Zhou X, Wu H, Zhang G, Shi T, Chen W. H19 promotes aerobic glycolysis, proliferation, and immune escape of gastric cancer cells through the microRNA-519d-3p/lactate dehydrogenase A axis. Cancer Sci 2021;112:2245-2259. https://doi.org/10.1111/cas.14896
29. Nian F, Qian Y, Xu F, Yang M, Wang H, Zhang Z. LDHA promotes osteoblast differentiation through histone lactylation. Biochem Biophys Res Commun, 2022;615:31-35. https://doi.org/10.1016/j.bbrc.2022.05.028
30. Yang W, Wang P, Cao P, Wang S, Yang Y, Su H, Nashun B. Hypoxic in vitro culture reduces histone lactylation and impairs pre-implantation embryonic development in mice. Epigenetics Chromatin, 2021;14:57. https://doi.org/10.1186/s13072-021-00431-6
31. Mezhibovsky E, Knowles KA, He Q, Sui K, Tveter KM, Duran RM, Roopchand DE. Grape polyphenols attenuate diet-induced obesity and hepatic steatosis in mice in association with reduced butyrate and increased markers of intestinal carbohydrate oxidation. Front Nutr 2021;8:675267. https://doi.org/10.3389/fnut.2021.675267
32. Gao R, Li Y, Xu Z, Zhang F, Xu J, Hu Y, Yin J, Yang K, Sun L, Wang Q, He X, Huang K. Mitochondrial pyruvate carrier 1 regulates fatty acid synthase lactylation and mediates treatment of nonalcoholic fatty liver disease. Hepatology 2023;78:1800-1815. https://doi.org/10.1097/HEP.0000000000000279
33. Yu J, Chai P, Xie M, Ge S, Ruan J, Fan X, Jia R. Histone lactylation drives oncogenesis by facilitating m 6 A reader protein YTHDF2 expression in ocular melanoma. Genome Biol 2021;22:85. https://doi.org/10.1186/s13059-021-02308-z

34. Yang Y, Cai J, Yang X, Wang K, Sun K, Yang Z, Zhang L, Yang L, Gu C, Huang X, Wang Z, Zhu X. Dysregulated m6A modification promotes lipogenesis and development of non-alcoholic fatty liver disease and hepatocellular carcinoma. Mol Ther 2022;30:2342-2353. https://doi.org/10.1016/j.ymthe.2022.02.021
35. Peng Z, Gong Y, Wang X, He W, Wu L, Zhang L, Xiong L, Huang Y, Su L, Shi P, Cao X, Liu R, Li Y, Xiao H. METTL3-m(6)A-Rubicon axis inhibits autophagy in nonalcoholic fatty liver disease. Mol Ther 2022;30:932-946. https://doi.org/10.1016/j.ymthe.2021.09.016
36. Piccinin E, Cariello M, De Santis S, Ducheix S, Sabbà C, Ntambi JM, Moschetta A. Role of oleic acid in the gut-liver axis: from diet to the regulation of its synthesis via stearoyl-coa desaturase 1 (SCD1). Nutrients 2019;11:2283. https://doi.org/10.3390/nu11102283
37. Mauvoisin D, Mounier C. Hormonal and nutritional regulation of SCD1 gene expression. Biochimie 2011;93:78-86. https://doi.org/10.1016/j.biochi.2010.08.001
38. Stoffel W, Schmidt-Soltau I, Jenke B, Binczek E, Hammels I. Hair growth cycle is arrested in SCD1 deficiency by impaired wnt3a-palmitoleoylation and retrieved by the artificial lipid barrier. J Invest Dermatol 2017;137:1424-1433. https://doi.org/10.1016/j.jid.2017.02.973
39. Shi H, Wei J, He C. Where, When, and How: Context-dependent functions of RNA methylation writers, readers, and erasers. Mol Cell 2019;74:640-650. https://doi.org/10.1016/j.molcel.2019.04.025
40. Liu T, Wei Q, Jin J, Luo Q, Liu Y, Yang Y, Cheng C, Li L, Pi J, Si Y, Xiao H, Li L, Rao S, Wang F, Yu J, Yu J, Zou D, Yi P. The m6A reader YTHDF1 promotes ovarian cancer progression via augmenting EIF3C translation. Nucleic Acids Res 2020;48:3816-3831. https://doi.org/10.1093/nar/gkaa048
41. Anita R, Paramasivam A, Priyadharsini JV, Chitra S. The m6A readers YTHDF1 and YTHDF3 aberrations associated with metastasis and predict poor prognosis in breast cancer patients. Am J Cancer Res 2020;10:2546-2554.
42. Lin Z, Niu Y, Wan A, Chen D, Liang H, Chen X, Sun L, Zhan S, Chen L, Cheng C, Zhang X, Bu X, He W, Wan G. RNA m(6) A methylation regulates sorafenib resistance in liver cancer through FOXO3-mediated autophagy. EMBO J 2020;39:e103181. https://doi.org/10.15252/embj.2019103181